Available online at www.sciencedirect.com
SCIENCE DIRECT®
ELSEVIER
Journal of Magnetism and Magnetic Materials 261 (2003) 328–336
journal of magnetism and magnetic materials
www.elsevier.com/locate/jmmm

Influence of Zr and Nb dopant additions on the microstructure and magnetic properties of nanocomposite $RE_2(Fe,Co)_{14}B/\alpha(Fe,Co)$ (RE = Nd–Pr) alloys

I. Betancourt[a,*], H.A. Davies[b]

[a] *Institute for Materials Research, UNAM. PO Box 70-360, Mexico DF, 04510 Mexico*
[b] *Department of Engineering Materials, University of Sheffield, Mappin St, Sheffield, S1 3JD, UK*

Received 7 March 2002; received in revised form 6 May 2002

Abstract

Nanocomposite REFeB alloy ribbons based on Nd/Pr rare earth (RE) mixtures were produced by devitrification of amorphous melt spun alloys. The effect of Zr and Nb dopant additions on the microstructures and magnetic properties of two-phase $RE_2Fe_{14}B/\alpha$-Fe alloy ribbons are reported, the aim being to refine the α-Fe grain size with the refractory metal addition through retardation of the crystal growth rate. For the Zr-containing alloys ($RE_yFe_{94-y-z}Zr_zB_6$, $y = 8, 10, z = 0-4$) only modest improvements of the magnetic properties, in comparison with the Zr-free alloys, were achieved for 8 at% RE ribbon while, for 10% RE 2% Zr ribbon, fairly good combinations of intrinsic coercivity ${}_iH_c$ (~ 400 kA/m) and maximum energy product $(BH)_{max}$ (~ 130 kJ/m^3) were achieved. Improved grain refinement was achieved with the Nb addition, though the magnetic properties were broadly comparable with those for Zr doped alloys. Both Zr and Nb doping, however, resulted in a steep decrease in Curie temperature, reflecting an attenuation of the exchange interactions in the 2/14/1 unit cell. Additional substitution of 10% of the Fe by Co for the Nb doped alloy resulted in enhanced T_c, more than compensating for the reduction due to the Nb, and resulting also in an excellent combination of ${}_iH_c$ (~ 500 kA/m) and $(BH)_{max}$ (140 kJ/m^3).

PACS: 75.50.Ww; 75.50.Tt

Keywords: Nanocomposite; Remanence enhancement; Dopant additions

1. Introduction

Since the nanocomposite $RE_2Fe_{14}B/Fe_3B$ and $RE_2Fe_{14}B/\alpha$-Fe melt spun alloys were first reported by Coehoorn et al. [1] and by Manaf et al. [2], respectively, this type of permanent magnet has received considerable attention [3–12]. The main characteristic of these so-called exchange spring magnets is the exchange coupling between magnetically hard and soft phases so that the magnetisation and anisotropy of the composite represent some average of the respective values for the constituent phases [13] and that the remanence J_r is enhanced above the value of $J_s/2$ (where J_s is the saturation polarisation), expected on the basis

*Corresponding author. Institute for Materials Research, UNAM. PO Box 70-360, Mexico DF, 04510 Mexico. Fax: +52-55-56161-371.
E-mail address: israelb@correo.unam.mx (I. Betancourt).

0304-8853/03/$ - see front matter
PII: S0304-8853(02)00366-9

of the Stoner–Wolfarth theory of non-interacting, uniaxial, single domain particles [14]. For this coupling to be effective, the mean size of the soft grains d_g^s, should not exceed a small multiple of the wall width δ_B for the hard phase (i.e. ~ 15 nm). In this way, the hard grains serve to stiffen the magnetisation of the whole material to such an extent that, in the second quadrant of the J–H loop, the hard grains do not easily reverse and the magnetisation of the soft phase is reversible [13]. Therefore, the d_g^s, as well as the mean diameter of the hard phase grains d_g^h, are important parameters to be controlled in order to achieve good magnetic properties. This does not represent a major problem, in principle, for nanocrystalline alloys produced by direct quenching from the liquid state, for which the high cooling rate facilitates very large undercoolings and very high nucleation frequencies for both $RE_2Fe_{14}B$ and α-Fe crystallites, thus yielding fine grained structures. The main practical impediment is the narrow process window and the tendency to produce a range of ribbon thicknesses in a batch and thus with variable microstructure and properties [15].

An obvious method of overcoming this limitation is "overquenching" to the fully amorphous state followed by a devitrification anneal. This has been shown to give broadly comparable microstructures and magnetic properties for stoichiometric $RE_2Fe_{14}B$ alloys to those obtained by direct quenching [11,22]. However, for initially amorphous REFeB materials (overquenched) with Fe-rich compositions (RE content <11.7 at%) the microstructural evolution on annealing starts with the precipitation and growth of α-Fe grains [10,16,17] followed by the formation and growth of the $RE_2Fe_{14}B$ crystallites. This process tends to result in a coarse microstructure of $RE_2Fe_{14}B$ grains and especially of α-Fe grains which deteriorates substantially the magnetic properties of composite structure [5,9,10,17].

However, the addition of small concentrations of refractory elements (such as Zr or Nb) have been reported as being useful in controlling the grain size of both the α-Fe and 2/14/1 phases in NdFeB [18–20] and in PrFeB [9,12,21,22] nanocrystalline alloys and hence, in improving the magnetic property enhancement relative to the ternary overquenched and annealed NdFeB/PrFeB alloys.

In addition, previous studies on single phase stoichiometric (Nd/Pr)FeB alloys [11,23–25] have shown the advantage of partial substitution of Nd by Pr, since it leads to higher intrinsic coercivities, afforded by the higher anisotropy field H_A of the PrFeB phase relative to NdFeB, without a significantly adverse effect on enhancement of the remanent polarisation J_r and with only a small reduction in the Curie temperature T_c [11]. In any case, the T_c reduction can be compensated for by partial substitution of Fe by Co. Thus, the present paper presents the results of a study of the microstructures and magnetic properties of mixed rare earth (Nd/Pr)(Fe,Co)B nanocomposite alloys and of the influence of dopant additions of Zr or Nb. The Nd:Pr ratio (3:1) was chosen to be close to that occurring in many natural rare earth ores, which is of particular interest from the viewpoint of possible reduced cost commercial exploitation.

2. Experimental

Ingots of the alloys were prepared using commercial grade materials by arc-melting the constituents in a high purity Ar atmosphere. The compositions of the alloys were $(Nd_{0.75}Pr_{0.25})_y$-$Fe_{94-y-z}Zr_zB_6$ $(y = 8, 10, z = 0, 1, 2, 3, 4)$; $(Nd_{0.75}$-$Pr_{0.25})_8Fe_{86-w}Nb_wB_6$ $(w = 0, 1.5, 2.5, 3.5)$, and $(Nd_{0.75}Pr_{0.25})_y(Fe_{0.9}Co_{0.1})_{91.5-y}Nb_{2.5}B_6$ $(y = 8, 10)$. The ingots were fragmented and melt spun in an Ar atmosphere at 0.5 atm pressure using a roll speed of 45 m/s in order to provide fully amorphous ribbons which was verified by X-ray diffraction (XRD). The alloy samples were devitrified by heat treating at 700°C for 10 min in sealed silica tubes previously evacuated and backfilled with Ar. XRD traces of samples of selected as-spun ribbons and of all the devitrified ribbons were obtained using a Philips 1710 X-ray diffractometer with Co K_α radiation. The microstructure of selected samples were investigated by transmission electron microscopy using a Philips 400 TEM, with thin foils prepared by ion-beam thinning. The magnetic properties of individual lengths of

ribbons, of typical mass 20 mg, were measured across the width (perpendicular to the casting direction and in the ribbon plane) and averaged for 8 ribbon pieces per alloy, using a vibrating sample magnetometer coupled to a 5 T superconducting magnet. Curie temperatures were determined by differential scanning calorimetry in a Dupont DSC instrument at a heating rate of 40°C/min.

3. Results and discussion

3.1. Zr-containing alloys

The X-ray diffractograms after annealing for $(Nd_{0.75}Pr_{0.25})_8Fe_{86-z}Zr_zB_6$ ($z = 0-4$) are shown in Fig. 1. The peak at $2\theta = 52.5°$, corresponding to the (1 1 0) α-Fe reflection is attenuated with increasing Zr content, which, according to previous reports [18,19] is due to the formation of a Zr-rich phase which also enhances the (2 2 1) reflection at $2\theta = 34.5°$ (presumably Zr_3Fe). The remaining peaks can be ascribed to the $RE_2Fe_{14}B$ phase. For 4% Zr alloys, a considerable decrease in the peak intensities reflects the significant dilution of the 2/14/1 phase at this Zr concentration. The TEM microstructure of selected 8 and 10 at% RE Zr-free and 10 at% RE Zr-containing alloys are shown in Fig 2. Some very large grains, in excess of 100 nm, and having internal microstructure (dislocation-like features) are observed for the $(Nd_{0.75}Pr_{0.25})_8Fe_{86}B_6$ alloy (Fig. 2a), evidently corresponding to the α-Fe phase, while some others (very small) do not show inner structure at all, which may be consequence of being 2/14/1 grains. This microstructure is in marked contrast to the ultra fine grained structure observed for the corresponding directly quenched nanocomposite alloy in which d_g for the 2/14/1 and α-Fe phases of 30 and <15 nm, respectively were observed [2]. Similar coarse microstructures, especially of the α-Fe constituent, have been observed previously in both NdFeB and PrFeB overquenched and annealed nanocomposite alloys [5,9,10,17].

Fig. 2b shows the microstructure of a $(Nd_{0.75}Pr_{0.25})_{10}Fe_{84}B_6$ ribbon alloy. In spite of a generally finer grain size distribution than for the 8 at% RE ribbon, including some grains with d_g of about 25 nm, some large grains ($d_g > 50$ nm) are still present which adversely affect the exchange coupling between hard and soft grains.

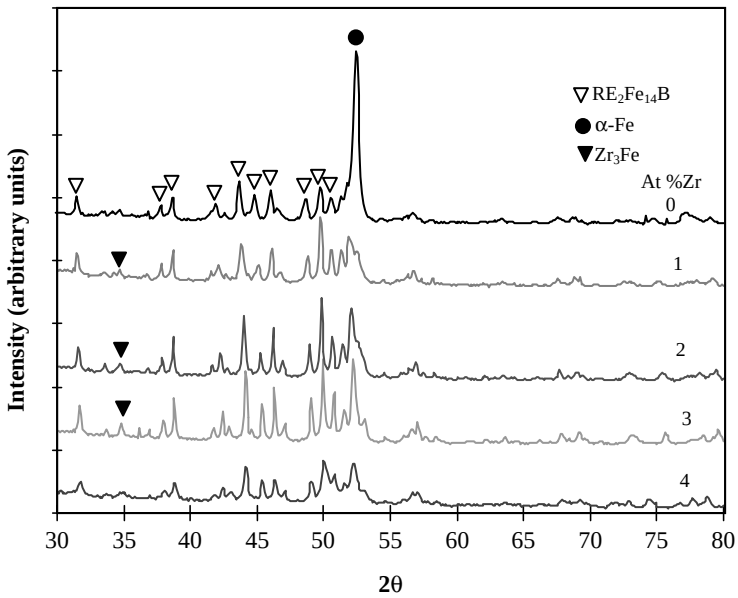

Fig. 1. X-ray diffractograms for ribbons in the $(Nd_{0.75}Pr_{0.25})_8Fe_{86-z}Zr_zB_6$ ($z = 0-4$) alloy series.

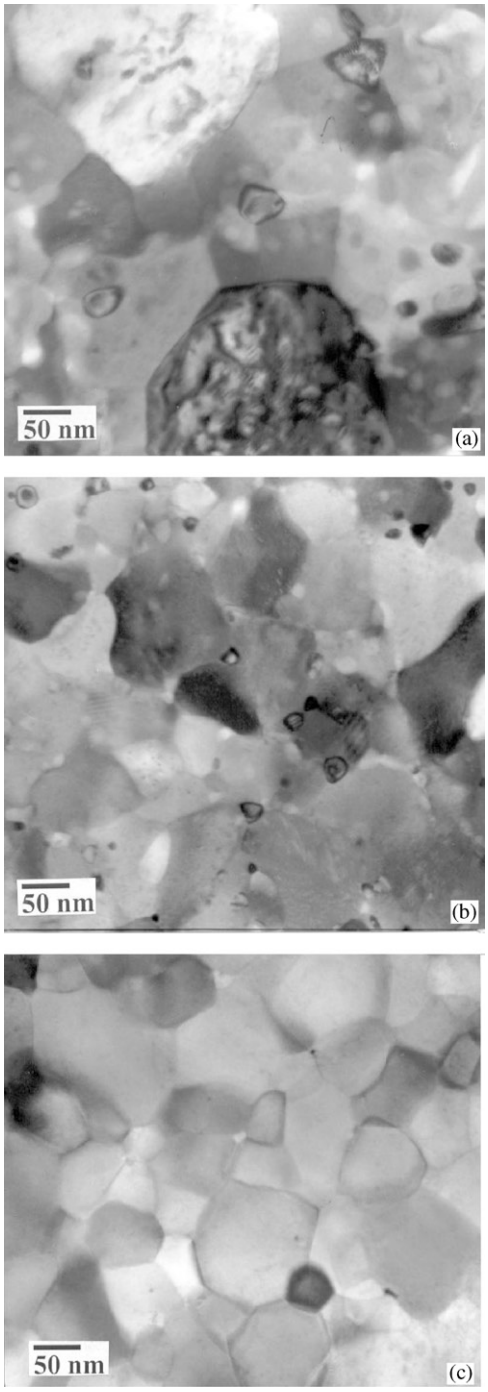

Fig. 2. TEM micrographs of (a) $(Nd_{0.75}Pr_{0.25})_8Fe_{86}B_6$ alloy ribbons, (b) $(Nd_{0.75}Pr_{0.25})_{10}Fe_{84}B_6$ alloy ribbons, (c) $(Nd_{0.75}Pr_{0.25})_{10}Fe_{82}Zr_2B_6$ alloy ribbons.

Fig. 2c shows a TEM micrograph of a $(Nd_{0.75}Pr_{0.25})_{10}Fe_{82}Zr_2B_6$ alloy ribbon, which indicates now the absence of coarse α-Fe crystallites; the grain size distribution is unimodal, suggesting a retarding of the crystal growth rate for α-Fe by the Zr but, nevertheless, the mean grain diameter appears to be not significantly different from that for the Zr-free alloy shown in Fig. 2b.

The magnetic properties of $(Nd_{0.75}Pr_{0.25})_y$-$Fe_{94-y-z}Zr_zB_6$ ($y = 8, 10$; $z = 0-4$) are shown in Fig. 3. For the 8%RE, Zr-free alloy (Fig. 3a), the rather poor combination of properties ($J_r = 0.9$ T, ${}_iH_c = 250$ kA/m and $(BH)_{max} = 67$ kJ/m^3) is considered to be a consequence of the coarse microstructure, notably of the α-Fe (>100 nm) grains, which significantly reduces the exchange coupling

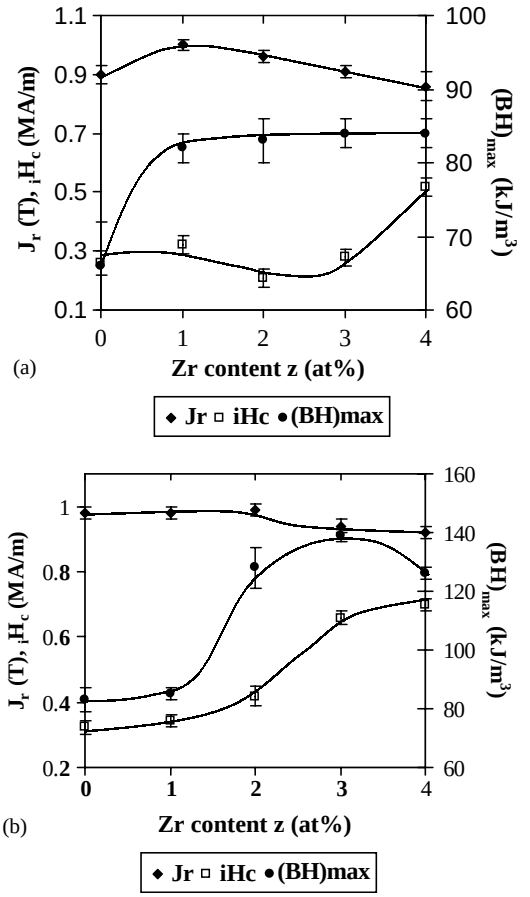

Fig. 3. Magnetic properties of ribbons in the alloy series $(Nd_{0.75}Pr_{0.25})_yFe_{94-y-z}Zr_zB_6$ ($z = 0-4$): (a) $y = 8$, (b) $y = 10$.

between hard and soft magnetic phases and results in no significant enhancement of J_r above the value of 0.9 T calculated on the basis of a volume average for the two component phases. In this state, the magnetisation reversal of the soft phase occurs independently, which has a detrimental effect on the shape of the second quadrant of the J–H loop (Fig. 4). For the Zr-containing alloy ribbons ($z = 1-4$), J_r attains a maximum at 1 at% Zr, and then decreases linearly for higher Zr contents. The coercivity appears to decrease slightly on first adding Zr but then increases beyond ~ 3 at% Zr. $(BH)_{max}$ is significantly improved with addition of Zr but is constrained by the small ${}_iH_c$ at low Zr while, at higher Zr, the reduced J_r is the constraining factor. Thus, for this high α-Fe volume fraction 8 at% RE alloy, the Zr additions do not give enhanced properties overall.

For the 10 at% RE alloy (Fig. 3b) a more useful effect of the Zr additions on the magnetic properties is observed because of a more effective grain refining effect, with d_g being typically ~ 50 nm, although no apparent difference is evident between d_g^s and d_g^h i.e., the grain diameter appears to have a unimodal distribution. This reduces the volume fraction of material exchange coupled between the two phases, in comparison with directly quenched alloys since, according to micromagnetic calculations [26], d_{g^s} should be about one half the d_{g^h} in order to ensure optimum exchange coupling between the two phases. This reduced exchange coupling is reflected in moderately enhanced J_r (~ 0.98 T) up to 2% Zr and a slight decrease at higher Zr concentrations. ${}_iH_c$, on the other hand, increases with Zr concentration, particularly at higher Zr, consistent with an expected enhancement of the anisotropy field [27]. Thus, considerable improvements to above 400 kA/m at 2 at% Zr and to >650 kA/m for 3 at% Zr are observed. These enhanced ${}_iH_c$ and J_r result in useful $(BH)_{max}$ enhancements above 125 kJ/m^3, with a maximum value of 139 kJ/m^3 at 3 at% Zr.

There is, however, a significant penalty; the Curie temperature of the hard 2/14/1 phase for the composite $(Nd_{0.75}Pr_{0.25})_yFe_{94-y-z}Zr_zB_6$ ($y = 8, 10$; $z = 0-4$) ribbons is plotted in Fig. 5 as a function of the Zr concentration z. The decrease in T_c with increasing Zr is consistent with the assumption that Zr enters the 2/14/1 lattice and influences its intrinsic magnetic properties, as indicated for H_A above. The plots for the 8 and 10 at% RE series in Fig. 5 also suggest that Zr enters the 2/14/1 phase preferentially since the rate of decrease of T_c with Zr content is steeper for the 8 at% RE than for 10 at% RE ribbons.

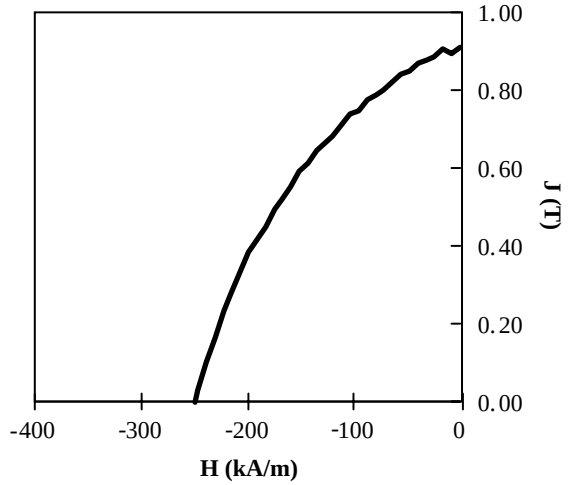

Fig 4. Demagnetising curve for a $(Nd_{0.75}Pr_{0.25})_8Fe_{86}B_6$ alloy ribbon.

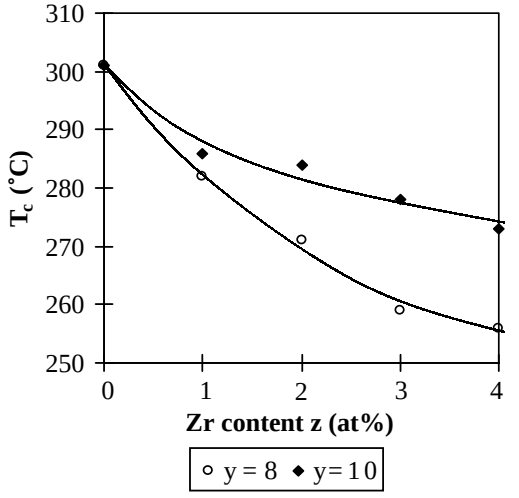

Fig. 5. Curie temperature of the hard 2/14/1 phase for the $(Nd_{0.75}Pr_{0.25})_yFe_{94-y-z}Zr_zB_6$ ($y = 8, 10$; $z = 0-4$) alloy ribbon series.

3.2. Nb-containing alloys

X-ray diffractograms for the $(Nd_{0.75}Pr_{0.25})_8Fe_{86-w}Nb_wB_6$ ($w = 0, 1.5, 2.5, 3.5$) alloy series are shown in Fig. 6. In contrast to the Zr additions, Nb substitutions up to 2.5 at% preserve the α-Fe (1 1 0) reflection at $2\theta = 52.4^\circ$, though with progressively reduced relative intensity, and there is no evidence of other phases apart from the major 2/14/1 constituent. At Nb = 3.5 at%, however, the formation of a different phase is evident, since the intensities of all the 2/14/1 reflections are substantially reduced. The major peaks at $2\theta = 43^\circ$, 50°, 56.3° can be ascribed to either Fe_2Nb or to FeNb [28] together with α-Fe (at 52.4°) and a reduced proportion of 2/14/1 phase.

The microstructure of a selected $(Nd_{0.75}Pr_{0.25})_8Fe_{83.5}Nb_{2.5}B_6$ ribbon is shown in Fig. 7. Unlike their Zr-containing counterparts, these Nb substituted alloys exhibit a largely homogeneous microstructure with no evidence of giant α-Fe grains and confirming the role of Nb as a crystal growth inhibitor. The mean grain diameter distribution, obtained from three different TEM micrographs and measuring individual grain dimensions along random diagonals, is bimodal, centred around 30 and 50 nm, corresponding to the α-Fe and the 2/14/1 phases, respectively. These mean grain sizes are broadly comparable with, but somewhat coarser than, those observed in directly quenched ternary NdFeB alloys [2].

The magnetic properties of the $(Nd_{0.75}Pr_{0.25})_8Fe_{86-w}Nb_wB_6$ ($w = 0, 1.5, 2.5, 3.5$) alloys are shown in Fig. 8. J_r is enhanced to above 1 T for all Nb contents, and much improved over the ternary alloys, reflecting the reduction in d_g promoted by the Nb addition. $_iH_c$ also increases considerably compared with the Nb-free alloy up to the range 350–400 kA/m for the 1.5 and 2.5 at% Nb ribbons. The trend of $(BH)_{max}$ with Nb content is similar to that of the coercivity, because of the dominant role of the $_iH_c$ over J_r on $(BH)_{max}$ for these low $_iH_c$, high Fe:RE ratio alloys. $(BH)_{max}$ values up $\sim 120\,kJ/m^3$ are observed for the 1.5 and 2.5 at% Nb ribbons. Beyond 2.5 at% Nb, the formation of the FeNb phase induces a collapse of both $_iH_c$ and $(BH)_{max}$. The Curie temperature of the $RE_2Fe_{14}B$ phase for $(Nd_{0.75}Pr_{0.25})_8Fe_{86-w}Nb_wB_6$ ($w = 0, 1.5, 2.5, 3.5$) alloy ribbons is plotted in Fig. 9. A sharp reduction in T_c is observed with increasing Nb content (similar in magnitude to that induced by Zr), which reflects the detrimental effect on the magnetic exchange interaction arising from the incorporation of Nb atoms into the 2/14/1 unit cell.

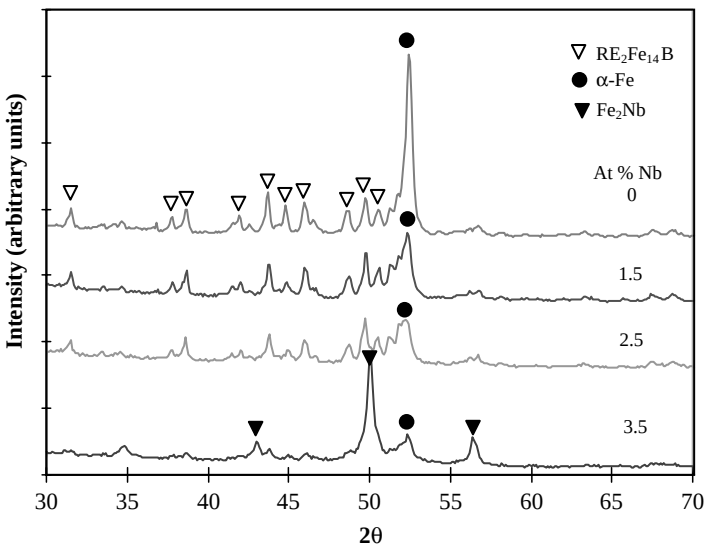

Fig. 6. X-ray diffractograms for the $(Nd_{0.75}Pr_{0.25})_8Fe_{86-w}Nb_wB_6$ ($w = 0, 1.5, 2.5, 3.5$) alloy ribbon series.

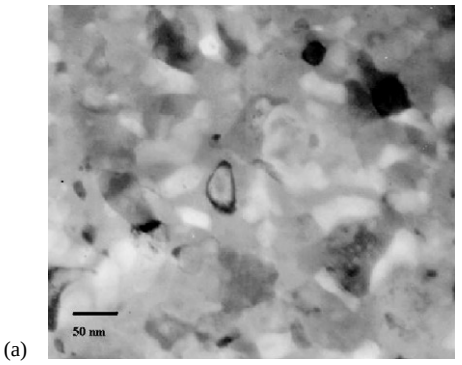

(a)

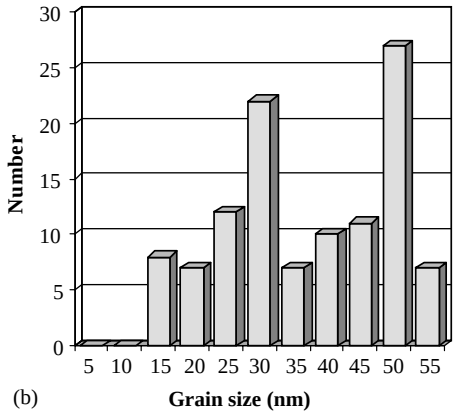

(b)

Fig. 7. (a) TEM micrograph of a selected $(Nd_{0.75}Pr_{0.25})_8Fe_{83.5}Nb_{2.5}B_6$ alloy ribbon and (b) its corresponding grain size distribution.

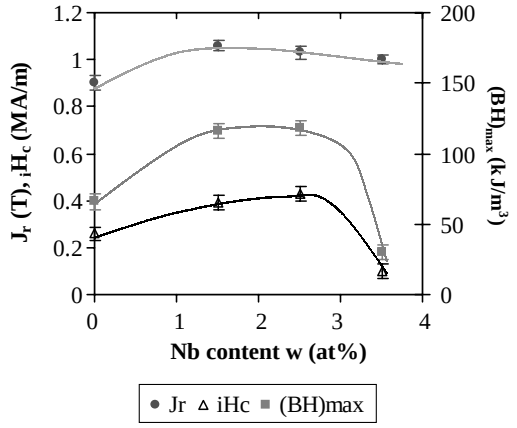

Fig. 8. Magnetic properties of ribbons in the $(Nd_{0.75}Pr_{0.25})_8Fe_{86-w}Nb_wB_6$ ($w = 0, 1.5, 2.5, 3.5$) alloy series.

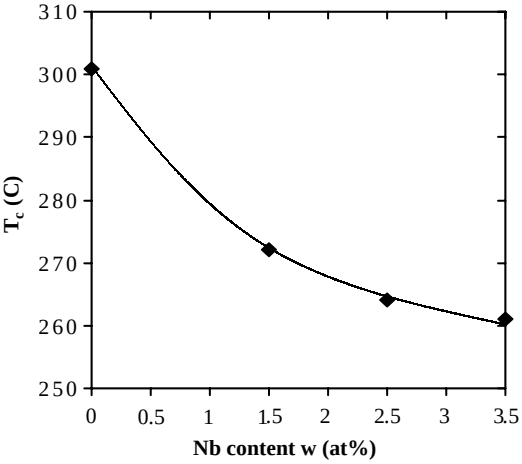

Fig. 9. Curie temperature of the $RE_2Fe_{14}B$ phase for $(Nd_{0.75}Pr_{0.25})_8Fe_{86-w}Nb_wB_6$ ($w = 0, 1.5, 2.5, 3.5$) alloy ribbons.

In order to compensate for the marked reduction in T_c caused by the Nb additions, 10% Co substitution for Fe in Nb-containing (2.5%) alloys was investigated. The magnetic properties of the (NdPr)(Fe,Co,Nb)B ribbons are shown in Fig. 10; specifically, data for $(Nd_{0.75}Pr_{0.25})_yFe_{94-y}B_6$, $(Nd_{0.75}Pr_{0.25})_yFe_{91.5-y}Nb_{2.5}B_6$, and $(Nd_{0.75}Pr_{0.25})_y(Fe_{0.9}Co_{0.1})_{91.5-y}Nb_{2.5}B_6$ are included for $y = 8$ and 10 at%. For 8 at% RE ribbons, J_r for the Co substituted alloys exhibits excellent enhancement in comparison with the Co-free compositions up to 1.16 T, at least partly due to the higher J_s of the $RE_2(Fe, Co)_{14}B$ phase [6]. In contrast, $_iH_c$ shows a slight decrease of $\sim$3%, compared with the Co-free ribbon, consistent with the reduction of H_A caused by the Co substitution [29]. However, it also leads to a marked deterioration of the squareness of the demagnetising curve (Fig. 11), which restricts $(BH)_{max}$ to moderate values of about 117 kJ/m^3. For the 10 at% RE ribbon, J_r is again substantially enhanced (1.09 T), in combination with good coercivity ($\sim$500 kA/m), which is surprisingly unaffected by the Co substitution. Thus, combined with excellent squareness of the second quadrant of the J–H loop (Fig. 11), this results in a large $(BH)_{max}$ of 140 kJ/m^3. The dependence of T_c on RE content for the 2/14/1 phase of this series of alloy ribbons is shown in Fig. 12. The considerable decrease in T_c with Nb

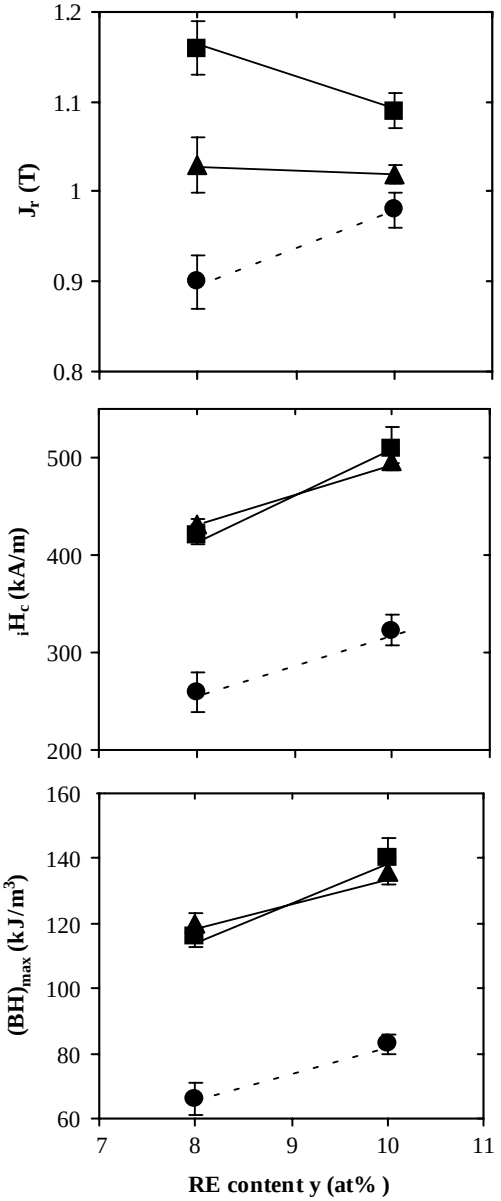

Fig. 10. Magnetic properties of the $(Nd_{0.75}Pr_{0.25})_y(Fe_{1-x}Co_x)_{94-y-w}Nb_wB_6$ ($y = 8, 10$) alloy series for: (i) $x = 0$, $w = 0$ (●); (ii) $x = 0, w = 2.5$ (▲); (iii) $x = 0.1, w = 2.5$ (■).

addition (as indicated in Fig. 9), is more than compensated by the fact that T_c is enhanced by $\sim 100^\circ$C for the 10% Co substitution for Fe, which is in accord with previous reports (Yapp and Davies [30]).

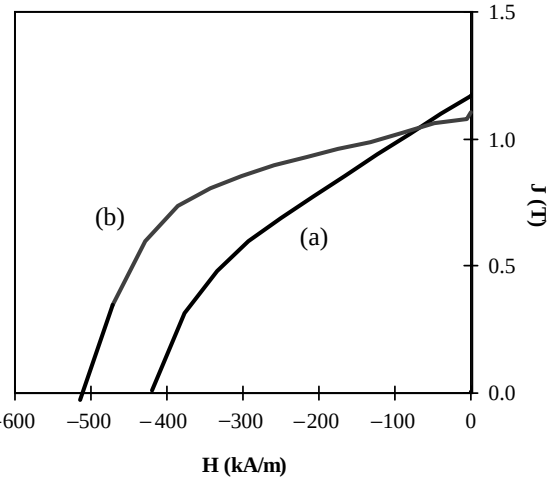

Fig. 11. Demagnetisation curves for $(Nd_{0.75}Pr_{0.25})_y(Fe_{0.9}Co_{0.1})_{91.5-y}Nb_{2.5}B_6$ alloy ribbons for (a) $y = 8$, (b) $y = 10$.

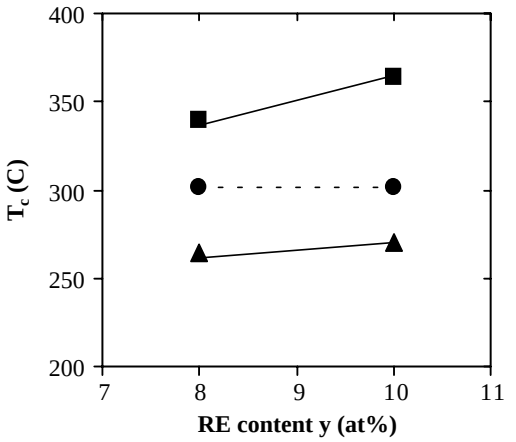

Fig. 12. Dependence on RE content of T_c for the 2/14/1 phase for $(Nd_{0.75}Pr_{0.25})_y(Fe_{1-x}Co_x)_{94-y-w}Nb_wB_6$ alloy ribbons for the following cases: (i) $x = 0, w = 0$ (●); (ii) $x = 0, w = 2.5$ (▲); (iii) $x = 0.1, w = 2.5$ (■).

4. Conclusions

Nanocomposite $(Nd_{0.75}Pr_{0.25})_yFe_{94-y}B_6$-based alloys ribbons processed by overquenching to the amorphous state, followed by a devitrification anneal, show moderate improvement of magnetic properties on substitution of dopant concentrations of Zr for Fe. However, the intrinsic coercivity $_iH_c$ is rather low, notably because of large α-Fe grains (typically > 50 nm) whose growth

was not retarded sufficiently by the Zr addition. Nb substitutions, on the other hand, resulted in improved ${}_{\mathrm{i}}H_{\mathrm{c}}$ as a consequence of fine microstructure compared with the dopant-free and Zr-containing counterparts in particular through improved control of the α-Fe grain growth. Additional partial substitution of 10% Fe by Co leads to further enhancements of J_{r} and $(\mathrm{BH})_{\max}$, notably for the 10 at% RE alloy, together with substantial increase of the Curie temperature to a level (360°C) well above that for ternary NdFeB alloy. Thus, the $(\mathrm{Nd}_{0.75}\mathrm{Pr}_{0.25})_y(\mathrm{Fe}_{0.9}\mathrm{Co}_{0.1})_{91.5-y}\mathrm{Nb}_{2.5}\mathrm{B}_6$ ($y = 8, 10\%$) alloy is a promising candidate nanocomposite alloy for processing by the overquench/anneal route.

Acknowledgements

IJBR acknowledges the award of a research scholarship by DGAPA, UNAM, Mexico. The financial support for research on nanophase magnetic alloys at the University of Sheffield by the Engineering and Physical Sciences Research Council, through the Advanced Magnetics Programme, is gratefully acknowledged.

References

[1] R. Coehoorn, D.B. de Mooij, C. de Waard, J. Magn. Magn. Mater. 80 (1989) 101.
[2] A. Manaf, R.A. Buckley, H.A. Davies, J. Magn. Magn. Mater. 128 (1993) 302.
[3] L. Withawanasam, G.C. Hadjipanayis, R.F. Krause, J. Appl. Phys. 75 (1994) 6646.
[4] A. Inoue, A. Takeuchi, A. Makino, T. Masumoto, IEEE Trans. Magn. 31 (1995) 3626.
[5] W. Chang, D.M. Hsing, J. Appl. Phys. 79 (1996) 4843.
[6] J.F. Liu, H.A. Davies, J. Magn. Magn. Mater. 157/158 (1996) 29.
[7] I. Panagiotopoulos, L. Withanawasam, G.C. Hadjipanayis, J. Magn. Magn. Mater. 152 (1996) 353.
[8] L.H. Lewis, V. Panchanathan, in: L. Schultz, K.H. Muller (Eds.), Proceedings of the 15th International Workshop on RE Magnets and their Applications, MATINFO, Frankfurt, 1998, p. 233.
[9] Z. Chen, Y. Zhang, Y. Ding, G.C. Hadjipanayis, J. Appl. Phys. 85 (1999) 5908.
[10] Z. Wang, S. Zhou, M. Zhang, Y. Quiao, R. Wang, J. Appl. Phys. 86 (1999) 7010.
[11] H.A. Davies, C.L. Harland, J.I. Betancourt R, G. Mendoza, in: M. Coey et al. (Eds.), Proceedings of the MRS Symposium on Advanced Hard and Soft Magnetic Materials, Warrendale, USA, 1999, p. 27.
[12] Y.Q. Wu, D.H. Ping, K. Hono, M. Hamano, A. Inoue, J. Appl. Phys. 87 (2000) 8658.
[13] E. Kneller, R. Hawig, IEEE Trans. Magn. 27 (1991) 3588.
[14] E.C. Stoner, E.P. Wohlfarth, Philos. Trans. R. Soc. 240 (1948) 599.
[15] H.A. Davies, in: C.A.F. Manwaring, et al., (Eds.), Proceedings of the Eighth Symposium on Magnetic Anisotropy and Coercivity in RE-TM Alloys, University of Birmingham, UK, 1994, p. 465.
[16] Z. Wang, S. Zhou, M. Zhang, Y. Quiao, X. Gao, Q. Zhao, R. Wang, W. Gong, J. Appl. Phys. 85 (1999) 4880.
[17] A. Kojima, F. Ogiwara, A. Makino, A. Inoue, T. Masumoto, Mater. Sci. Eng. A 226–228 (1997) 520.
[18] O. Kohmoto, T. Yoneyama, K. Yajima, Jpn. J. Appl. Phys. 26 (1987) 1804.
[19] K. Yajima, H. Nakamura, O. Kohmoto, T. Yoneyama, J. Appl. Phys. 64 (1988) 5528.
[20] H. Chiriac, M. Marinescu, K.H.J. Buschow, F.R. de Boer, E. Bruck, J. Magn. Magn. Mater. 203 (1999) 153.
[21] D. Goll, H. Kronmuller, in: L. Schultz, K.H. Muller (Eds.), Fifteenth International Workshop on RE Magnets and their Applications, MATINFO, Frankfurt, 1998, p. 189.
[22] C.L. Harland, H.A. Davies, J. Appl. Phys. 87 (2000) 6116.
[23] M. Seeger, D. Kohler, H. Kronmuller, J. Magn. Magn. Mater. 130 (1994) 165.
[24] L.H. Lewis, V. Panchanathan, J. Wang, J. Magn. Magn. Mater. 176 (1997) 288.
[25] J.I. Betancourt R, H. A. Davies, J. Appl. Phys. 85 (1999) 5911.
[26] R. Fischer, J. Schrefl, H. Kronmuller, J. Fidler, J. Magn. Magn. Mater. 153 (1996) 35.
[27] M. Jurczyk, W.E. Wallace, J. Magn. Magn. Mater. 59 (1986) L182.
[28] M. Leonowicz, A. Manaf, H.A. Davies, Mater. Lett. 14 (1992) 279.
[29] R. Grossinger, R. Krewenka, X.K. Sun, E. Eibler, H.R. Kirchmayr, K.H.J. Buschow, J. Less-Common Met. 124 (1986) 165.
[30] R. Yapp, H.A. Davies, in: L. Schultz, K.-H. Muller (Eds.), Proceedings of the 15th International Workshop RE Magnets and their Applications, MATINFO, Frankfurt, 1998, p. 315.